Fluid dynamic analysis of a cryogenic piston pump

Fluid dynamic analysis of a cryogenic piston pump

Stefano Cioni[1,*], Francesco Balduzzi[1], Luca Romani[1], Alessandro Bianchini[1] and Giovanni Ferrara[1]

[1]Department of Industrial Engineering (DIEF), Università degli Studi di Firenze, Via di Santa Marta 3, 50139 Firenze, Italy

*Corresponding author: stefano.cioni@unifi.it

Abstract. Cryogenic piston pumps are commonly found in cryogenic systems to pressurize low-temperature liquefied fuels, such as liquified natural gas (LNG) or hydrogen, which are then gasified and stored in high-pressure vessels. The main challenges to be tackled in the design of these machines concern the low operating temperatures, high discharge pressures, and especially the need to avoid liquid evaporation, as this can lead to a reduction of volumetric efficiency or even to the shutdown of the pump. Two effects can cause the formation of vapor bubbles: cavitation, i.e., when the static pressure falls below the saturation value during the suction phase, and evaporation due to a temperature increase of the cryogenic liquid.
In this study, a numerical analysis of a cryogenic single-piston pump is carried out. In the first part of the activity, the suction phase is studied through three-dimensional, steady-state CFD simulations. The performance of the pump in terms of pressure losses is evaluated and possible improvements to the suction geometry are identified.
Then, two-phase steady-state Eulerian-Eulerian simulations are performed. The Rayleigh-Plesset model is used in order to evaluate the onset of cavitation. The minimum inlet pressure conditions that avoid cavitation are identified for two different geometries underlining the positive effect of the introduced modifications. Results show that the methodology applied in this work can lead to improvements in cryogenic pump design, reducing the static pressure losses and hence limiting the risk of cavitation.

1. Introduction

The cryogenic piston pump is a crucial component of any cryogenic system, either to mobilize or pressurize the working fluid. Long-distance transport of liquified natural gas (LNG) represents the most common application in the energy sector, since this technology allows a reduction of transport costs over long distances, due to the increase in volumetric density compared to the compressed gas solutions [1].

Similarly, as the transition to more sustainable fuels takes place, the same technology could be applied to the supply chain of hydrogen. In this context, multiple solutions are currently under analysis, especially for the automotive and transportation industries [2,3]. Vehicles could store hydrogen either as a compressed gas or as a cryogenic liquid, in order to increase the volumetric density. In the former case, hydrogen transported over long distances as a cryogenic liquid could be compressed and then gasified, hence reducing compression costs. Otherwise, in the latter case, refill of liquid hydrogen vehicles might take place in either low-pressure vessels or high-pressure (up to 350 bar), cryo-

compressed ones, which have been developed to reduce boil-off losses [3]. In these systems, the crucial component is represented by the piston pump, which needs to provide adequate efficiency and reliability.

The design of cryogenic pumps must address multiple challenges [4]. Firstly, these machines elaborate a liquid that is stored in cryogenic vessels in saturation conditions. The low temperature of the liquified gas is maintained by letting part of the fluid evaporate. The boil-off gas is then expelled from the vessel in order to maintain the pressure constant. Hence, since the liquid at the pump suction is close to saturation conditions, these machines must reduce internal losses to limit the risk of cavitation. Secondly, the heat transfer with the external ambient must be minimized, both to reduce the formation of vapor bubbles, which can lead to the shutdown of the pump, and to minimize the loss of cryogenic liquid, which reduces the efficiency of the system. Finally, the low temperatures and high pressures (up to 400 bar) require an accurate design and selection of materials, in order to guarantee adequate reliability.

Previous works on cryogenic pumps have focused on experimental tests of existing pumps.

Biermann and Kohl [5] performed tests on a five-cylinder, variable displacement piston pump by using both liquid hydrogen and nitrogen. No major differences in pump performance were observed when switching between the two liquids. The cavitation characteristic of the pump was analyzed by testing different rotational speeds.

Lue et al. [6] evaluated the characteristic curve of a single piston cryogenic pump developed to operate with liquid helium. It was observed that the volumetric efficiency of the pump is reduced at lower rotational speed due to fluid evaporation.

Yamane et al. [7] tested different piston geometries for a liquid hydrogen pump. The effect of heat generated by friction, heat transfer with the external ambient, and throttling of fluid in the clearance between piston and cylinder were estimated. Additionally, different piston geometries were tested to identify the best solution to reduce liquid leakage.

Despite the many challenges, cryogenic piston pumps are generally designed through standard practices, following the experience gathered by the industry over the years, while more advanced simulation tools, such as CFD, are still not regularly applied. Indeed, to the best of the author's knowledge, no literature has been published concerning the application of modern simulation tools to cryogenic reciprocating piston pumps.

The goal of this work is to evaluate the effect of different suction geometry features on the performance of a prototype cryogenic pump. The pump is designed for being installed in a thermosiphon tank arrangement (Figure 1), with the suction pipe connected to the bottom part of the cold-end. Single-phase, three-dimensional CFD simulations of the suction phase are carried out during the preliminary stages of design, to compare the effect of multiple geometry parameters on the pressure evolution along the suction path. Additionally, two-phase simulations are performed, and the onset of cavitation is analysed to evaluate the improvements reached with the best design obtained for the suction geometry.

This work is organized as follows. The tested geometry is described in Section 2, as well as the different parameters which were evaluated during this work. The methodology is described in Section 3 followed by a summary of the results in Section 4. Finally, the main conclusions and prospects are discussed in Section 5.

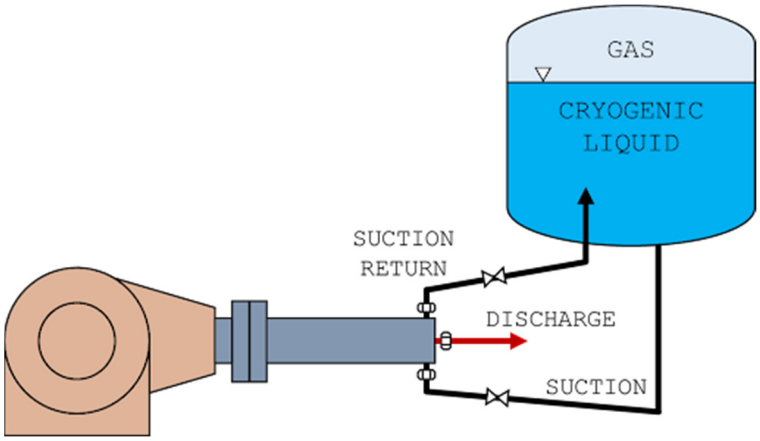

Figure 1. Cryogenic pump system

2. Pump Geometry

The simulations performed in this work are carried out on a cryogenic single piston pump model (Figure 2 shows a conceptual schematic). The pump is a prototype that is currently in the last phases of design, so, in order to guarantee confidentiality, a detailed representation of the geometry can not be provided.

The pump presents a suction duct, which fills an internal volume surrounding the cylinder body. This volume maintains the temperature of the cylinder at the working value for long periods of time, even after pump shut-down. Additionally, it guarantees the cooling of the pump, dissipating the heat generated due to friction between the piston rings and cylinder, thanks to the vaporization of a very small amount of cryogenic liquid that is allowed to flow back to the tank through the return piping. The pump is insulated by a vacuum jacket, which limits the heating of the fluid caused by the temperature difference with the external ambient.

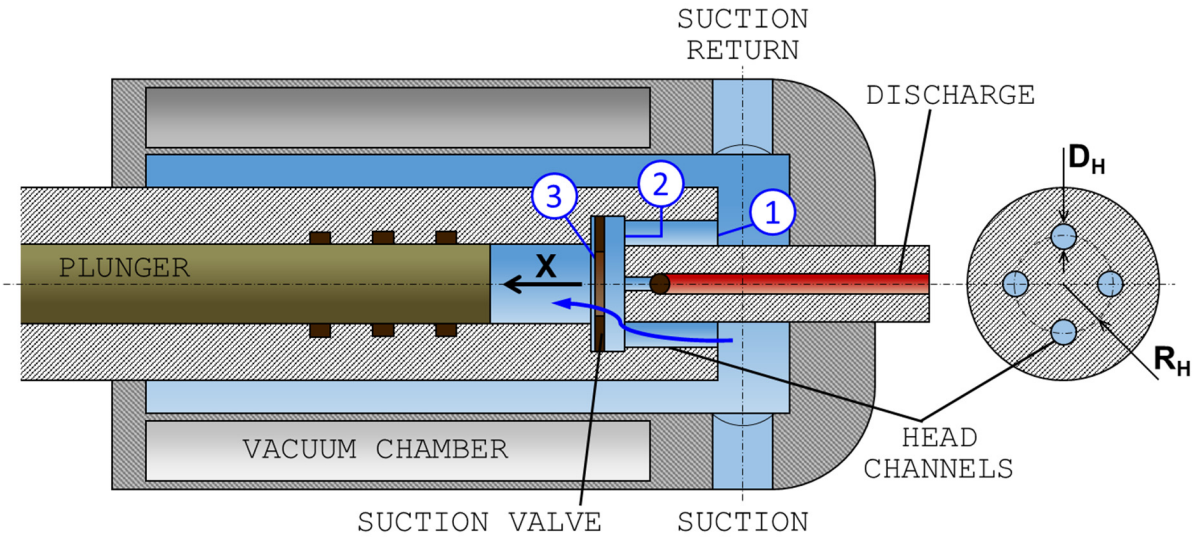

Figure 2. Cryogenic piston pump scheme. Sections 1,2 and 3 identify the head channels inlet and outlet and suction valve respectively.

The inner volume of liquid inside the pump feeds the compression chamber through multiple axial channels, located at the head of the cylinder. The channels are disposed along a circumference, surrounding the central discharge valve.

The automatic suction valve is a ring, pushed into position by the pressure differences between the cylinder and the outer volume.

The effect of multiple geometry parameters is tested. In detail, the effect of the head channels diameters (D_H), the number of head channels (N_H), and their radial position (R_H) are evaluated. The comparisons are carried out by modifying one parameter at a time, allowing the evaluation of the effect of each modification separately.

A summary of the tests performed is provided in Table 1. First, the effect of each parameter was tested independently by means of steady-state single-phase (liquid) simulations. The same inlet pressure was imposed for all the analyzed geometries to evaluate the difference in the pressure evolution along the suction path. The value of the inlet pressure was chosen to avoid reaching the saturation pressure in any point of the fluid domain. Second, two additional configurations were tested, namely: *Configuration A* (Average) which is defined by the average value of each parameter, and *Configuration B* (Best) which represents the combination of parameters providing the lowest value of pressure losses. For the two geometries *A* and *B*, additional two-phase simulations are run to analyse the onset of cavitation and to quantify the improvements reached by geometry *B*. In this case, the pressure imposed at the inlet boundary was not analogous for the two configurations, since the goal was indeed to find the minimum inlet pressure value, before undergoing cavitation.

3. Methodology

In this paragraph, a brief description of the simulation setup is provided for both single and multi-phase simulations.

The main objective when designing cryogenic piston pumps is to increase the minimum static pressure values, hence increasing the range of inlet pressures over which no cavitation occurs. The most critical part of the working cycle of the pump is the suction phase when the piston is moving towards the bottom dead center at its maximum velocity. At this point of the cycle, the liquid reaches the highest velocities and the lowest static pressure values.

Table 1. Test matrix of geometric parameters.

Configuration	D_H [mm]	N_H [-]	R_H [mm]	Total Channels Area [mm^2]
Diameter	6 7 8	10	16	282 384 502
Number	7	8 10 12	16	384
Radial Position	7	10	16 17 18 20	384
A	7	10	17	384
B	8	12	20	603

3.1. Single-phase simulations

Three-dimensional, steady-state RANS (Reynolds-Averaged Navier-Stokes) simulations are performed on the different geometry configurations shown in Section 2, by means of the commercial solver ANSYS CFX.

Liquid nitrogen is chosen as the working fluid so that results can be compared with future experimental campaigns. Indeed, liquid nitrogen represents the most common fluid employed for experimental tests, since it allows to reduce costs and minimize safety risks compared to liquified fuels such as LNG or liquid hydrogen.

The numerical set-up of the simulations was defined following previous works of some of the authors on the CFD analysis of suction pressure losses in reciprocating compressors [8,9]. During the definition of the numerical domain, the discharge ducts of the pump are excluded, since the focus of this work is the analysis of the suction losses and cavitation in the pump. A static pressure inlet is set at the inlet of the pump, which was extended by 5 diameters of the inlet duct to guarantee a fully developed flow. The outlet section is identified by the position of the piston at mid-stroke. Consequently, the outlet boundary condition is defined by setting the flow velocity equal to the maximum translational velocity of the piston.

The numerical domain was discretized through an unstructured mesh, which was generated automatically through the software ANSYS Meshing. Tetrahedral elements are used to discretize the core of the fluid domain. Local mesh refinements are introduced in the regions characterized by large velocity gradients. In particular, the mesh is refined inside the head channels and the cylinder, and further cell size reductions are imposed around the suction valve, as this region includes the choke section of the pump.

Orthogonal prismatic elements are used to discretize the large velocity gradients found inside the boundary layer. Twenty-four prismatic elements are used in the near wall region and the size of the first element is chosen in order to guarantee y^+<1 in the fluid domain. Mesh quality requirements were fulfilled in the transition region between the prismatic and tetrahedral elements by limiting the growth ratio to 1.1.

The shear stress transport (SST) method was chosen to close the RANS equations, as this turbulence model combines the main advantages of the k-ω and k-ε models[10]. This two-equation model is robust and no convergence issues are encountered across all the tested geometries.

3.2. Multi-phase simulations

From the results of the single-phase simulations, the best geometric configuration is identified, and it is compared with geometry *A* (Table 1). Additionally, the onset of cavitation is studied by performing Eulerian-Eulerian homogenous multi-phase simulations.

The mixture model is introduced to solve the multi-phase flow, which assumes that the two phases move at the same velocity, i.e. that the vapor bubbles are dispersed and transported by the liquid. The mass transfer between the phases is modeled through the Rayleigh-Plesset cavitation model [11], Equation (1),

$$\dot{m}_{\mathrm{fg}} = \frac{3 r_{\mathrm{g}} \rho_{\mathrm{g}}}{R_{\mathrm{B}}} \sqrt{\frac{2}{3} \frac{p_{\mathrm{v}} - p}{\rho_{\mathrm{f}}}}, \tag{1}$$

where $\dot{m}_{\mathrm{fg}}$ is the interphase mass flow rate from liquid to vapour due to cavitation, r_{g} is the volume fraction of the gas phase, R_B the mean bubble diameter, p_{v} is the saturation pressure and p and ρ_{f} are the pressure and density of the liquid, respectively. In this work, the mean bubble diameter, R_{B}, is assumed as $2e-6\ m$.

The interphase mass transfer is hence calculated from the static pressure of the liquid phase, knowing the saturation pressure at the liquid temperature. The saturation pressure was calculated from Antoine's Equation, Equation (2),

$$log_{10}p_{\mathrm{v}} = A - \frac{B}{C+T}, \tag{2}$$

where $A = 8.334$, $B = 588.725\ K$ and $C = -6.6\ K$, respectively.

The multi-phase simulations are performed by using the single-phase results as initial conditions, and by lowering the inlet pressure until the onset of cavitation.

4. Results

In this section, the results are presented. Firstly, Section 4.1 describes the single-phase results. The effects of the different geometric parameters on the fluid-dynamic performance of the pump are analysed. Then, the two configurations *A* and *B* are compared. It is worth pointing out that the inlet pressure for single-phase simulations was set to ensure that the local static pressure in the whole suction path does not fall below the saturation pressure. Secondly, Section 4.2, shows the two-phase simulation results, focusing on the analysis of cavitation occurrence. In these cases, the inlet pressure was progressively reduced from the original value, until the onset of cavitation was detected by the solver.

The results are presented in terms of the average total and static pressures and velocities for planes perpendicular to the axis of the piston and along the x coordinate (see Figure 2). The axial coordinate is normalized with the x coordinate of the computational domain (where "inlet" corresponds to the inlet section of the main suction duct, and "outlet" corresponds to the piston position at mid-stroke), Equation (3),

$$\boldsymbol{x} = \frac{x - x_{\mathrm{inlet}}}{x_{\mathrm{outlet}} - x_{\mathrm{inlet}}}. \tag{3}$$

The total and static pressures are normalized through the respective inlet values, Equations (4) and (5),

$$\boldsymbol{p_s} = \frac{p_{\mathrm{s}}}{p_{\mathrm{s,inlet}}}, \tag{4}$$

$$\boldsymbol{p_{tot}} = \frac{p_{\mathrm{tot}}}{p_{\mathrm{tot,inlet}}}, \tag{5}$$

and the velocity is normalized through the piston velocity, V_{p}, Equation (6),

$$\boldsymbol{V} = \frac{V}{V_{\mathrm{p}}}. \tag{6}$$

4.1. Single-phase suction analysis

The effect of the head channels diameters on the fluid-dynamic behaviour of the pump is shown in Figure 3. The axial location of the three most critical sections, defined in Figure 2, is also highlighted. The larger channel diameters, $D_{\mathrm{h}} = 8\ mm$, allows to reduce the total pressure losses during the suction phase (Figure 3 (a)). After the head channels inlet, the distributed losses along the ducts increase when the diameter is reduced. The liquid reaches higher velocities in order to achieve the same mass flow rate, and this results in lower static pressure values.

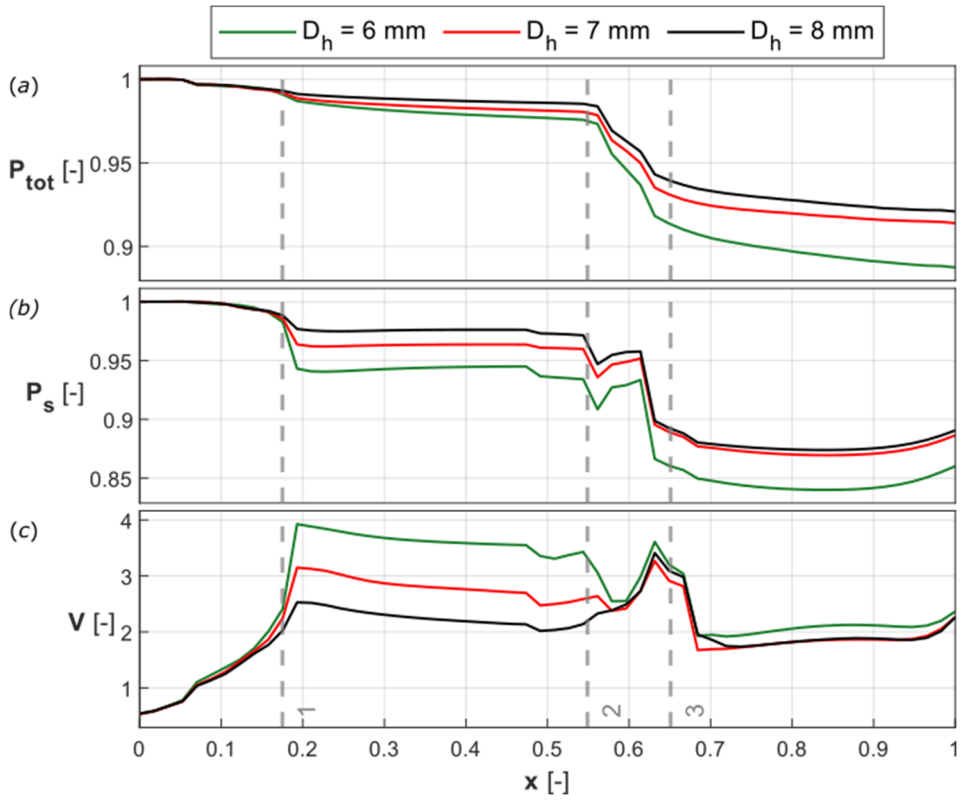

Figure 3 Performance comparison of cryogenic pump with varying diameters of the head channels.

After section 2 the three geometries behave in the same way, with similar total pressure losses and velocity profiles. Indeed, the choke section is the same for the three cases, and it is located at the lateral surface of the cylinder formed between the inner edge of the suction valve and the head of the cylinder. In the velocity plots, the choke section can be identified by the local velocity maximum found at $\boldsymbol{x} \approx 0.64$. The lowest static pressure values are reached in the $D_{\mathrm{h}} = 6\,mm$ configuration due to the high total pressure losses that take place in the head channels.

Figure 4 shows the effect of the number of head channels on the suction performance of the pump. Three different geometries are tested with eight, ten and twelve head channels respectively. The total section area is kept constant across the three cases in order to evaluate only the effect of the number of channels on the pump behavior.

In Figure 4 (a) it can be observed that the total pressure loss inside the head channels (between planes 1 and 2) is larger for the 8-channel configuration compared to the 10-channel one. This is due to the increased surface area of the second geometry, which causes an increase in total pressure losses. However, the same trend is not reflected in the results for the 12-channel geometry. Indeed, the latter configuration shows the minimum total pressure loss and highest static pressure values among the three cases. This might be caused by the reduced diameter of the head channels, which might not allow a free expansion of the separated boundary layer that is formed inside the channels. Hence, the actual available area of passage for the flow is larger for the 12-channel geometry, resulting in a reduced total pressure loss.

Indeed, Figure 5 shows the velocity fields for the three different configurations. Flow separation is more pronounced in the 10-channels geometry, and the liquid is forced to accelerate due to the reduced available cross section. Hence, this could be the cause of the increased pressure losses observed in Figure 4. Similar results can be observed for the 8-channel geometry. In contrast, in the 12-channel configuration, flow separation affects a limited length of the head channels, and the velocity recovers faster.

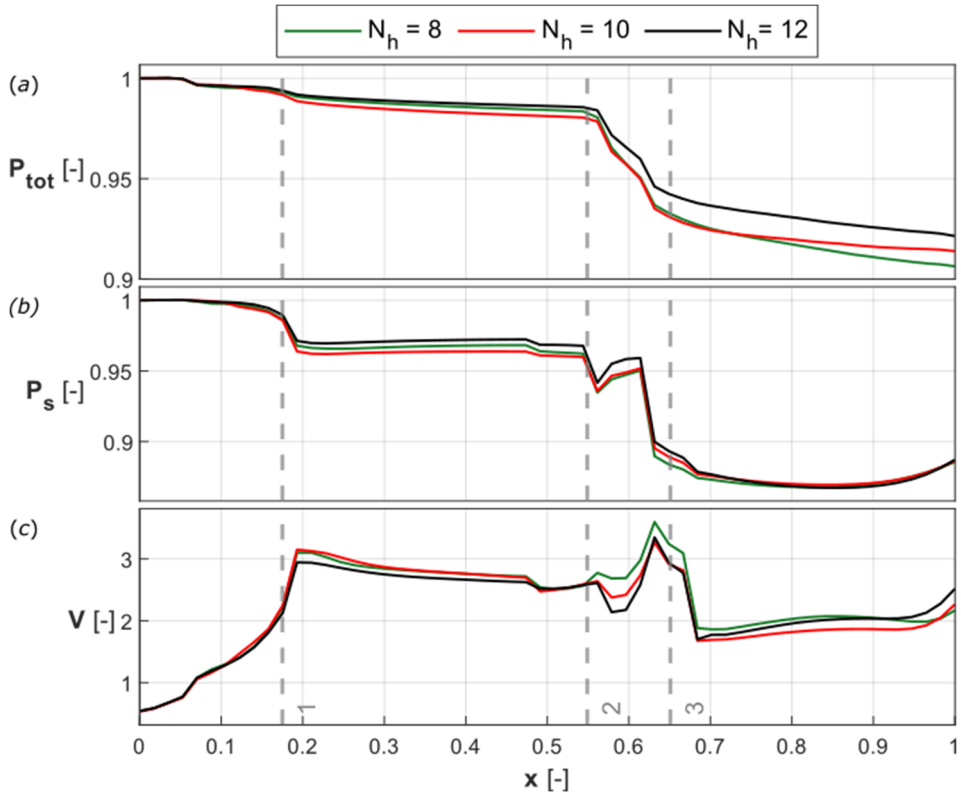

Figure 4. Performance comparison of the cryogenic pump with varying number of head channels. The total section area is constant for the three geometries.

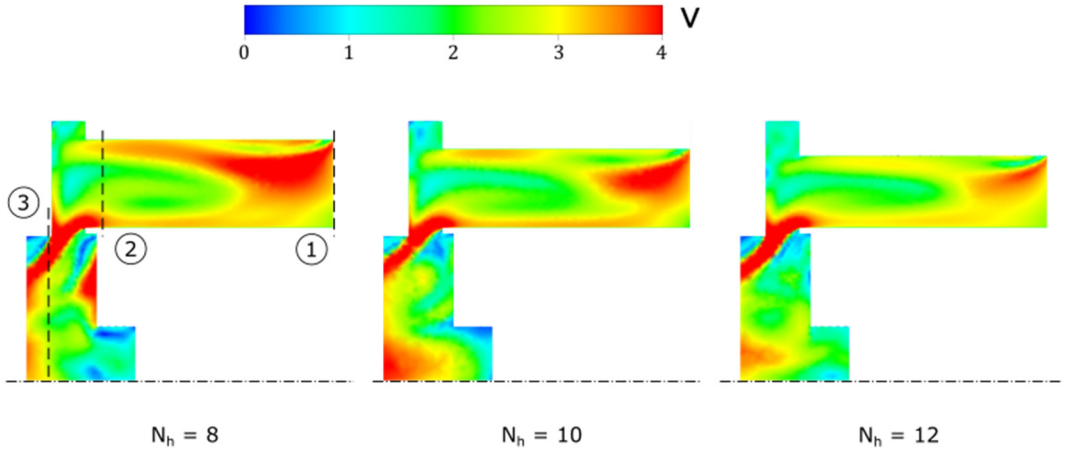

Figure 5. Velocity field for varying number of head channels.

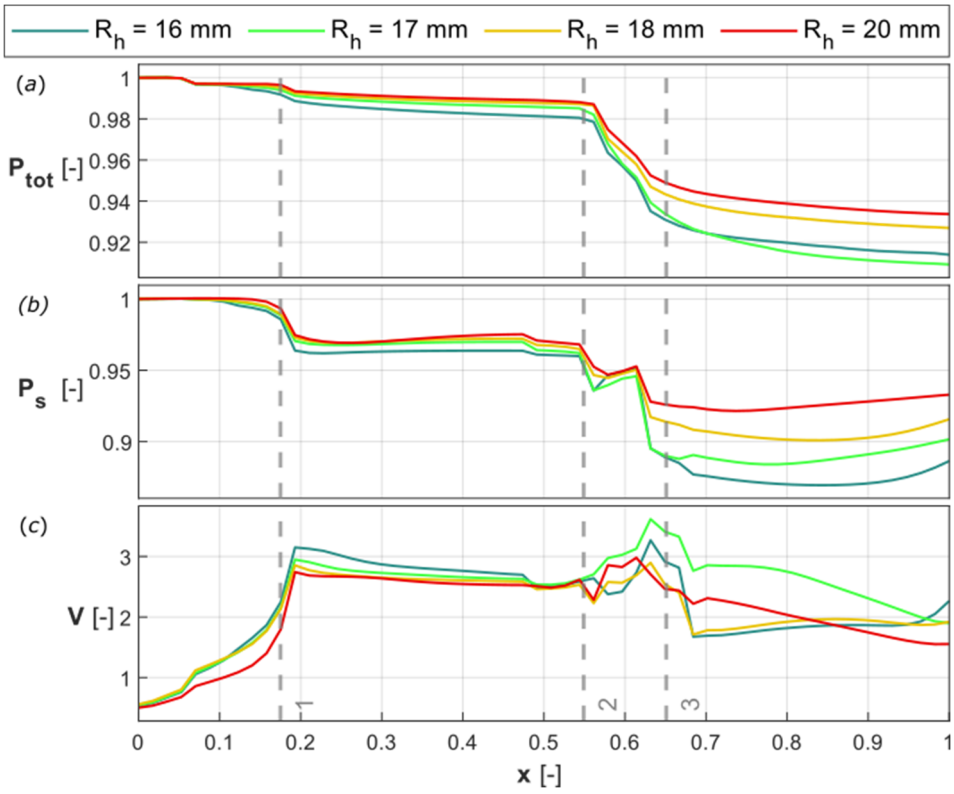

Figure 6. Performance comparison of cryogenic pump for increasing radial distance of head channels.

After the outlet of the head channels (Plane 2), the 12-channel geometry also shows a further reduction in total pressure losses. The increased number of channels might improve the distribution of the liquid inside the cylinder, resulting in a larger effective area available for the flow. Indeed, as it can be observed from Figure 4 (c), while the choke section is identical for the three geometries, the velocity reaches a lower value between planes 1 and 2 for the 12-channel configuration, at $\boldsymbol{x} \approx 0.59$ Despite this difference, the minimum average static pressure values are comparable across these three cases.

The effect of the radial distance of the head channels from the cylinder axis is shown in Figure 6. In this case, a difference in the results can be observed before the inlet of the head channels (plane 1). By increasing the radial distance, the total pressure losses are reduced, and the flow reaches larger static pressure values and lower velocities. This difference is caused by the disturbance introduced by the discharge valve.

The main difference between the test cases is observed after the outlet of the head channels (plane 2). The increased radial distance causes an increase in the choke section which results in an increase of the static pressure values. Moving from $R_{\mathrm{h}} = 16\,mm$ to $R_{\mathrm{h}} = 20\,mm$, the minimum average static pressure is increased by 9% Figure 6 (b)), while the total pressure drop is reduced by 22%. The average velocity trends, present a local maximum at $\boldsymbol{x} \approx 0.63\,mm$. However, the reduction of choke section does not seem to lead to a reduction in liquid velocities. This might be caused by the differences in the flow field at the outlet section of the head channels, for the different test cases. The separated boundary layer on the head of the cylinder can change the available cross-section for the liquid, hence influencing the velocity results.

Figure 7 shows a comparison between test cases *A* and *B* (see Table 1), which combine the geometric parameters that have been tested separately in the previous paragraphs. Case *B* shows the reduced total and static pressure losses during the suction phase, caused by the increased area of the head channels and the increased choke area. The total pressure loss is reduced by 44% while the average static pressure minimum is reduced by 50%. For both cases *A* and *B*, the choke section is identified by the lateral surface

of the cylinder formed between the suction valve edge and the head of the cylinder. Indeed, the velocity maximum is located at the same axial position $\boldsymbol{x} \approx 0.64$. The effect of the increased choke section can be observed, as the velocity maximum value is 3% higher for the *A* configuration.

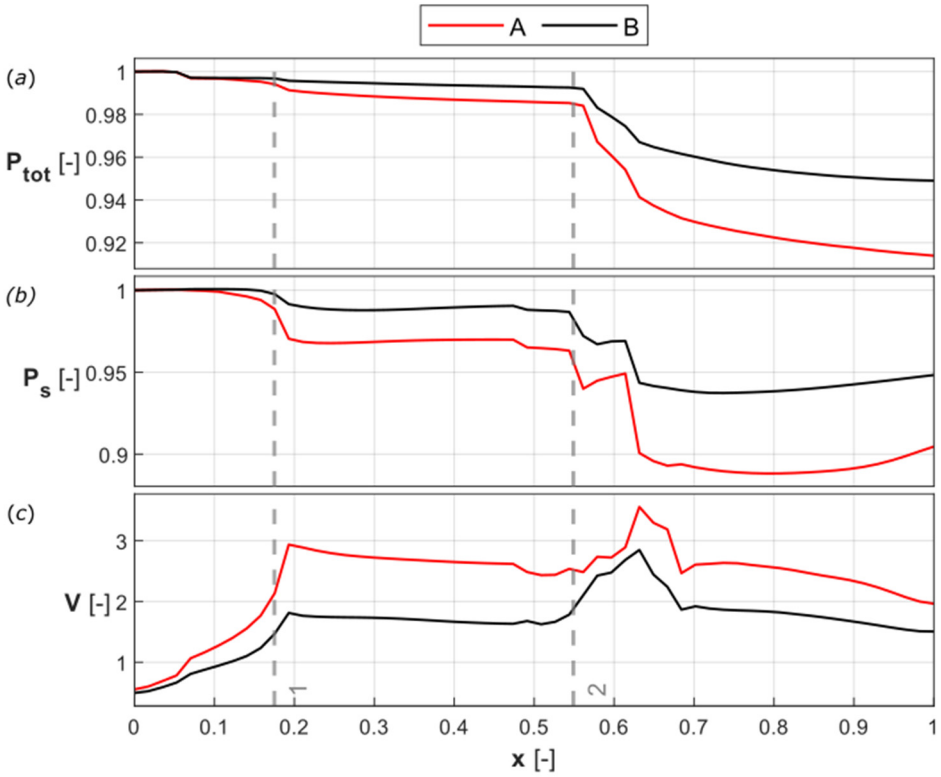

Figure 7 Fluid-dynamic comparison of configurations *A* and *B*.

4.2. Multi-phase simulations

As described in Section 3, multi-phase simulations of geometries *A* and *B* are performed. Figure 8 shows the static pressure results for the two configurations. In contrast to the previous figures, the static pressure trends are normalized with the inlet pressure value imposed for the single-phase simulations. Hence, the normalized static pressure value at $\boldsymbol{x} = 0$ represents the cavitation limit of each geometry. Vapor bubbles start forming after a reduction of 13% of the inlet static pressure for case *A* and of 19% for case *B*, showing the improvements achieved in terms of cavitation performance of the pump.

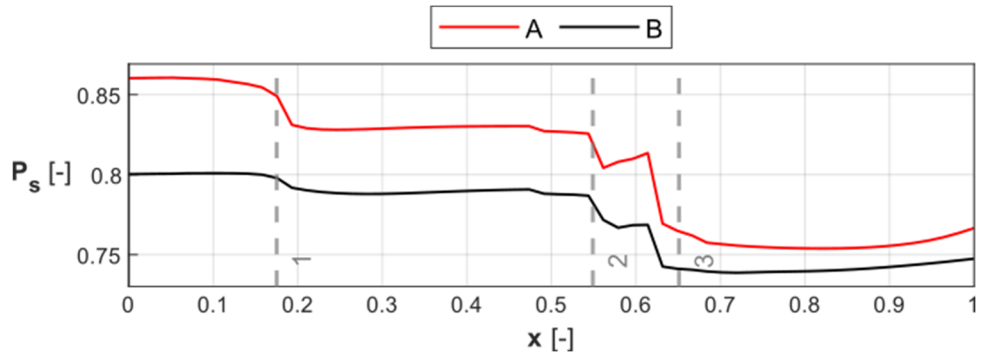

Figure 8. Average static pressure during pump cavitation for geometries *A* and *B*. Static pressure values normalized through the static inlet pressure value used for single-phase simulations.

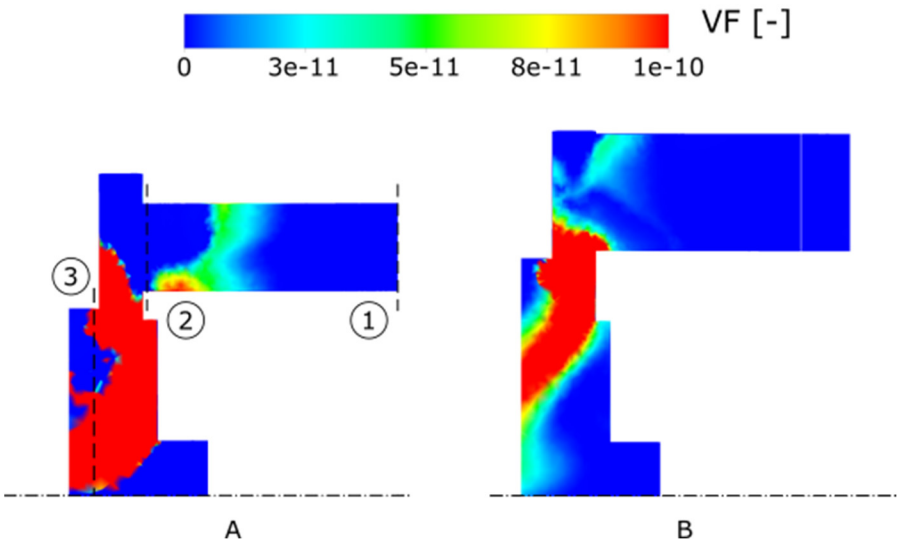

Figure 9. Nitrogen vapor volume fraction contours for geometry *A* (left) and *B* (right).

Figure 7 shows the vapor volume fractions contours for the two test cases. While the minimum average static pressures are observed inside the cylinder (see Figure 8), cavitation mainly takes place at the outlet of the head channels and around the choke section. In this part of the geometry, the liquid reaches the minimum local static pressure values, as it needs to accelerate through the choke section. Indeed, vapor bubbles are formed where the local static pressure falls below the liquid saturation pressure. In these terms, even though the minimum average static pressure values are 2% higher for configuration *A* compared to *B*, cavitation takes place in a larger area for case *A*. The main cause can be identified in the larger cross sections of geometry *B*, which lead to a reduced acceleration of the liquid and therefore, higher local static pressure values.

5. Conclusions

In this work, steady-state, single-phase, RANS simulations of a cryogenic reciprocating piston pump have been carried out. The main objective was to evaluate the effect of different modifications introduced in the suction geometry. Results showed that total and static pressure losses can be reduced by increasing the section of the head channels and the choke section. Additionally, increasing the number of head channels seemed to have only a limited effect on the static pressure values.

After analysing the effects of the various geometric parameters separately, a best-case scenario geometry was studied and compared with a non-optimized solution. The improvements led to a reduction of 44% and 50% of the total and static pressure losses, respectively.

Two-phase simulations of the improved geometry were carried out by adding the Rayleigh-Plesset cavitation model. The best design obtained for the suction geometry was capable of operating at lower inlet pressure values without the occurrence of cavitation.

In conclusion, the results show how high fidelity CFD analyses, carried out during the early stage of the design of a cryogenic piston pump, can support the definition of the final geometry. Crucial features in the prototype can be identified and optimised, leading to an increased range of operability of the pump. The improvements are introduced without the need of major modifications to the pump geometry which might require a re-design of the pump assembly and the verification of its structural integrity.

Future work might include performing unsteady simulations of the complete pump cycle, which could allow the analysis of unsteady effects altering the steady-state behaviour of the piston pump. Furthermore, steady state thermal simulations could be performed, in order to evaluate the formation of vapor bubbles due to heat transfer with the pump body.

References

[1] Economides M J, Sun K and Subero G 2006 Compressed Natural Gas (CNG): An Alternative to Liquefied Natural Gas (LNG) *SPE Production & Operations* **21** 318–24

[2] Zhang F, Zhao P, Niu M and Maddy J 2016 The survey of key technologies in hydrogen energy storage *International Journal of Hydrogen Energy* **41** 14535–52

[3] Satyapal S, Petrovic J, Read C, Thomas G and Ordaz G 2007 The U.S. Department of Energy's National Hydrogen Storage Project: Progress towards meeting hydrogen-powered vehicle requirements *Catalysis Today* **120** 246–56

[4] Brailovskii Ya L 2000 High-pressure pumps for cryogenic liquids: Problems and prospects *Chem Petrol Eng* **36** 90–3

[5] Biermann A E and Kohl R C 1959 *Preliminary Study of a Piston Pump for Cryogenic Fluids*

[6] Lue J W, Miller J R, Walstrom P L and Herz W 1981 *Test of a cryogenic helium pump* (Oak Ridge National Lab., TN (USA))

[7] Yamane K, Nakamura S, Nosset T and Furuhama S 1996 A study on a liquid hydrogen pump with a self-clearance-adjustment structure *International Journal of Hydrogen Energy* **21** 717–23

[8] Balduzzi F, Ferrara G, Babbini A and Pratelli G 2013 CFD Evaluation of the Pressure Losses in a Reciprocating Compressor: A Flexible Approach ASME 2012 11th Biennial Conference on Engineering Systems Design and Analysis (American Society of Mechanical Engineers Digital Collection) pp 63–72

[9] Balduzzi F, Ferrara G, Maleci R, Babbini A and Pratelli G 2014 A Parametric Computational Fluid Dynamics Analysis of the Valve Pocket Losses in Reciprocating Compressors *Journal of Pressure Vessel Technology* **137**

[10] Menter F R 1992 *Improved two-equation k-omega turbulence models for aerodynamic flows*

[11] Franc J-P 2007 The Rayleigh-Plesset equation: a simple and powerful tool to understand various aspects of cavitation *Fluid Dynamics of Cavitation and Cavitating Turbopumps* CISM International Centre for Mechanical Sciences ed L d'Agostino and M V Salvetti (Vienna: Springer) pp 1–41